JMEPEG (2018) 27:124–137
https://doi.org/10.1007/s11665-017-3090-z

1059-9495/$19.00

Characterization of Mechanical Properties and Residual Stress in API 5L X80 Steel Welded Joints

Amilton de Sousa Lins Jr., Luís Felipe Guimarães de Souza, and Maria Cindra Fonseca

(Submitted June 22, 2017; in revised form October 27, 2017; published online December 20, 2017)

The use of high-strength and low-alloy steels, high design factors and increasingly stringent safety requirements have increased the operating pressure levels and, consequently, the need for further studies to avoid and prevent premature pipe failure. To evaluate the possibility of improving productivity in manual arc welding of this type of steel, this work characterizes the mechanical properties and residual stresses in API 5L X80 steel welded joints using the SMAW and FCAW processes. The residual stresses were analyzed using x-ray diffraction with the $\sin^2\psi$ method at the top and root of the welded joints in the longitudinal and transverse directions of the weld bead. The mechanical properties of the welded joints by both processes were characterized in terms of tensile strength, impact toughness and Vickers microhardness in the welded and shot peening conditions. A predominantly compressive residual stress was found, and shot peening increased the tensile strength and impact toughness in both welded joints.

Keywords API 5L-X80 steel, mechanical properties, residual stresses, shot peening, welding, x-ray diffraction

1. Introduction

Natural resources such as oil and natural gas are often located in distant regions of consumer markets, which requires high operating pressures to increase the transport capacity. As a result, the need has grown for steels whose mechanical characteristics present high resistance and good formability to build pipelines with high security and reliability (Ref 1, 2).

The use of high-strength and low-alloy steels and increasingly stringent safety requirements have increased the pressure levels in operation. The large-diameter pipes in high-pressure pipelines are manufactured by welding; as is common in welded structures near the weld beads, it is the preferred location for the nucleation and propagation of cracks (Ref 2, 3). API 5L X80 is a high-strength low-alloy steel with low-carbon and high-grade steel; it is used in the manufacture of pipes for oil and gas transportation (Ref 2).

Welding is an essential process to assemble oil and gas pipelines over long distances under high pressures. During the conventional welding process of the pipes, some problems occur, such as the low mechanical resistance and toughness of the heat-affected zone. In addition, the steels that are used in the manufacture of the pipelines are susceptible to hydrogen-induced cracking when they are welded in conventional processes (Ref 4).

Amilton de Sousa Lins Jr., and **Maria Cindra Fonseca**, Departamento de Engenharia Mecânica/PGMEC, Universidade Federal Fluminense – UFF, Rua Passo da Pátria, 156, São Domingos, Niterói, RJ 24210-240, Brazil; and **Luís Felipe Guimarães de Souza**, CEFET/RJ – Departamento de Engenharia Mecânica, Avenida Maracanã, 229, Bolco E, Sala 506, Maracanã, Rio de Janeiro, RJ 20271-110, Brazil. Contact e-mail: mcindra@vm.uff.br.

Residual stresses are self-equilibrated stresses that remain in the material after the external agents that cause these stresses are removed. Most manufacturing processes produce a considerable amount of residual stresses, and their appearance in the welding is even more relevant due to the high thermal gradient, which is associated with the inherent plastic deformations and phase transformations of the process (Ref 3).

The fatigue resistance of metallic alloys depends highly on the residual stress state induced in the surface layers. It is well established that compressive residual stresses are beneficial to the fatigue life and stress corrosion and inhibit crack nucleation and propagation (Ref 5). An excellent method to introduce surface residual stresses to improve the fatigue life of materials is the shot peening mechanical process. However, the introduced residual stresses may be reduced or completely relieved when cyclic mechanical or thermal loads are applied (Ref 6). Although several studies present the influence of shot peening in the fatigue life of components, pipes and structures (Ref 7-11), there are few studies of the effect of shot peening on the mechanical properties of materials (Ref 12).

In the present study, welded joints of API 5L X80 grade line-pipe steel were obtained by the Shielded Metal Arc Welding (SMAW) and Flux Cored Arc Welding (FCAW) processes. Mechanical properties (hardness, mechanical strength and toughness) and the residual stress behavior of the joints with and without the shot peening mechanical treatment were analyzed and compared.

2. Materials and Methods

2.1 Materials

API 5L X80 steel plates, which were produced by controlled rolling, were welded using the Shielded Metal Arc Welding (SMAW) and Flux Cored Arc Welding (FCAW) processes. The chemical compositions of the steel and weld metals in both processes are shown in Tables 1 and 2, respectively.

Table 1 Chemical composition of API 5L X80 steel (% weight)

C	Si	P	S	Mn	Mo	Ni	Cu	Cr	Ti	V	C_{eq}
0.08	0.222	0.014	0.0014	1.74	0.117	0.014	0.019	0.166	0.015	< 0.001	0.429

Table 2 Chemical composition of the weld metals (% weight)

Weld metal	C	Si	P	S	Mn	Mo	Ni	Cu	Cr	Ti	V	C_{eq}
SMAW	0.064	0.284	0.0084	< 0.001	1.55	0.33	1.52	0.018	0.106	0.0046	0.018	0.513
FCAW	0.048	0.64	0.0091	0.0041	1.91	0.56	2.62	0.015	0.152	0.0027	0.018	0.688

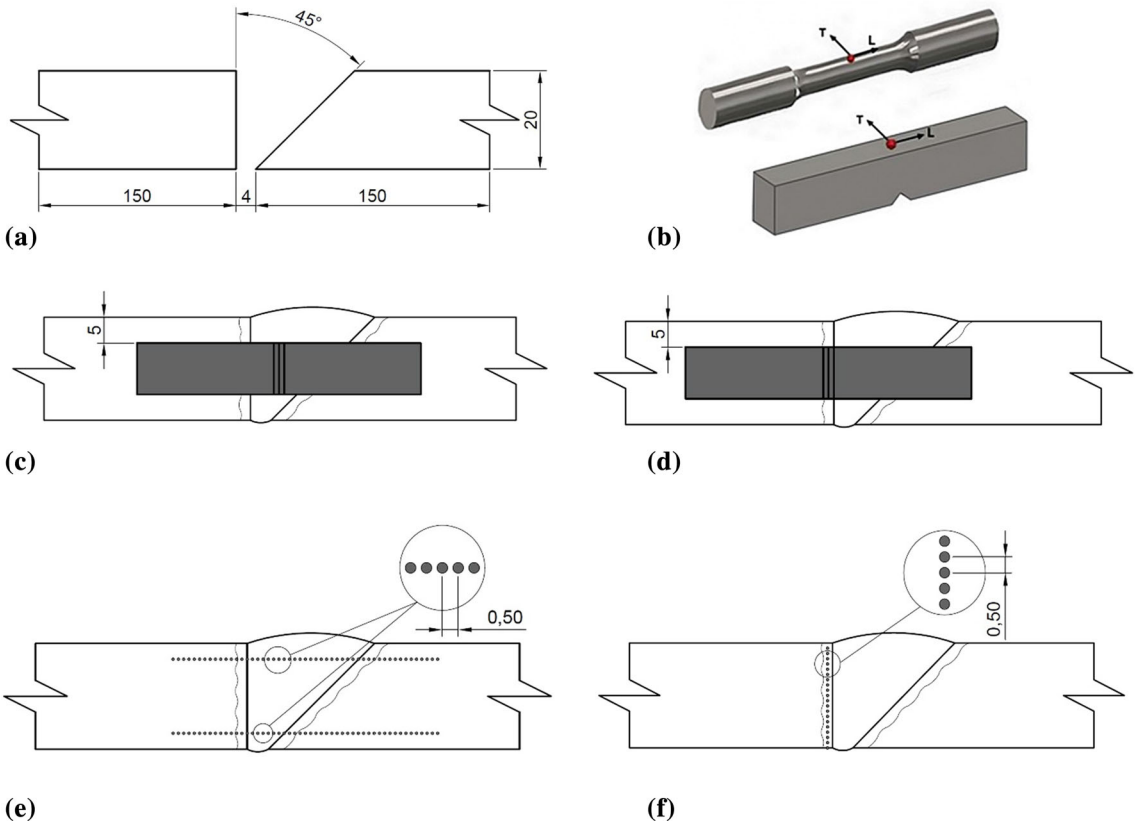

Fig. 1 (a) Details of the joint geometry (dimensions in mm), (b) residual stress analysis direction in tension and Charpy specimens, Location of the specimens for Charpy-V impact test and notch position: (c) on the weld metal and (d) on the HAZ, and Location of the Vickers microhardness test: (e) transverse measurements in the region of the weld joint and (f) measurements in the HAZ

2.2 Welding Joints

Plates with dimensions 300 × 150 × 20 mm were welded according to the geometry and dimensions in Fig. 1(a). Multipass welding in a flat position with preheating at 120 °C and a maximum interpass temperature of 150 °C was performed using the SMAW and FCAW processes. The preheating and interpass temperatures were controlled using a contact pyrometer.

Tables 3 and 4 show the average welding parameters. For the FCAW process, a mixture of 15% CO_2 and 85% Ar was used as the shielding gas with a flow rate of 18 L/min. The distance from the contact tip to the workpiece was 20 mm.

2.3 Shot Peening Mechanical Treatment

The shot peening mechanical treatment was performed in tensile and Charpy-V specimens according to SAE J442 (Ref 13) at an Almen intensity (A) of 0.25A using a glass shot with diameter of 0.59-0.71, coverage of 200%, distance between the blast nozzle and the test piece of 100 mm, pressure of 0.8 MPa, incident angle 90° and shot velocity 30 m/s.

2.4 Residual Stress Analysis

The surface residual stress was analyzed using the x-ray diffraction technique with the $\sin^2\psi$ method for which the lattice spacing d of material was measured at five ψ-angles

Table 3 Welding parameters of the SMAW process

Pass	Position	Diameter, mm	Current, A	Voltage, V	Time, s	Speed, mm/s	Welding energy, KJ/mm
1-2	Root	3.25	75-80	22-23	531	1.83	1.29
3-12	Filler	4.00	175-180	24-26	2925	3.26	1.15
13-16	Top	3.25	145-150	22-24	385	3.64	0.96
End					3841	2.91	1.13

Table 4 Welding parameters of the FCAW process

Pass	Position	Diameter, mm	Current, A	Voltage, V	Time, s	Speed, mm/s	Welding energy, KJ/mm
1-2	Root	1.2	148-152	23-24	347	2.76	1.61
3-8	Filler	1.2	204-224	25-27	525	4.26	1.40
9-12	Top	1.2	208-216	26-27	279	5.24	1.03
End					1151	4.09	1.35

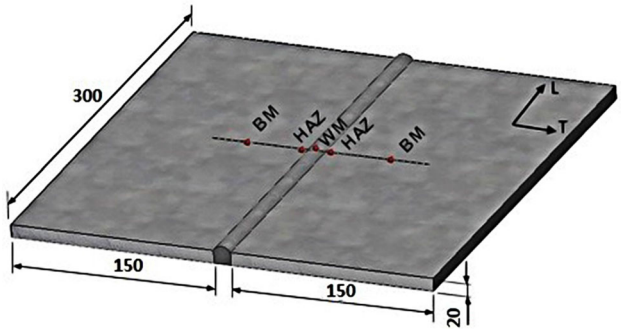

Fig. 2 Schematic representation of welded joint showing location (red points) and direction (L and T) of residual stresses measurement (dimensions in mm) (Color figure online)

between − 45° and + 45°. Based on a linear regression fit, the variations of 2θ versus $\sin^2\psi$ plots were recorded and the residual stress was evaluated. An accuracy of approximately 15 MPa was achieved using x-ray diffraction. The parameters are shown in Table 5. The stress was measured using a XStress3000 portable analyzer with a collimator of Ø 1.0 mm (30 kV and 6.7 mA). The XTronic V1-0 Standard software (stresstechgroup.com) was used for the stress calculation.

Figure 2 shows the regions of the weld joint where the residual stress measurements were taken: base metal (BM), heat-affected zone (HAZ) and weld metal (WM) in the longitudinal (*L*) and transverse (*T*) directions relative to the weld bead.

The residual stresses were measured in all tensile and Charpy specimens before the mechanical tests in the welded and shot peening conditions. The stress was measured in the longitudinal (*L*) and transverse (*T*) directions relative to the main axis of the specimens (Fig. 1b).

Before the residual stress measurements, the specimens were electrolytically polished to remove the oxide layer. Polishing was performed using a high ionic solution with an electrical potential and a current. A sodium chloride saturated solution with glycerin was used as the electrolyte, and the voltage and current parameters were 30 V and 0.20 A, respectively.

2.5 Mechanical Properties Characterization

The specimens for the mechanical property characterization were made according to the ASTM A370-05 (Ref 14) standard for the tensile tests; their gauge length and diameter were 50 and 8.75 mm, respectively. Tensile tests were performed in a universal tension testing machine (Instron 5985 model) with a 250-kN-capacity load cell and a testing speed of 3 mm/min at room temperature. A set of 3 specimens was used for each condition.

Charpy-V impact tests were performed at − 40, 0 and 25 °C in the specimens according to the ASTM A-370-05 (Ref 14) standard. The specimens were withdrawn transversely to the weld bead and 5 mm from the joint surface. The notch was positioned at the center of the weld metal, heat-affected zone (HAZ) and base metal. A set of 3 specimens was used for each condition. Figure 1(c) and (d) shows the position of the notch for the weld metal and HAZ.

Vickers microhardness tests were performed according to the ASTM A 370-05 (Ref 14) standard with an applied load of 1 kgf on the test specimens that were transverse to the weld metal. The test was performed at 3.0 mm from the surface and at the root of the weld joint, which covered the weld metal, HAZ and base metal. These tests were also performed in the HAZ along the thickness that corresponded to the position of the Charpy-V notch on the impact test specimens. A microhardness-testing machine Instron-Wilson, model 402 MVD, was used, and Fig. 1(e) and (f) shows the position of the hardness tests.

2.6 Metallographic Preparation

The metallographic examination was conducted on samples taken transversally to the weld bead. The samples were carefully ground with emery paper up to 1200 grid and polished using diamond paste with 6, 3 and 1 mm and etched with 2% nital solution. The microstructure was observed via scanning electron microscopy (SEM) in secondary electron mode on: top bead and columnar and reheated regions of the weld metal corresponding to the Charpy-V notch position. Also, some of the Charpy-V specimens fracture surfaces were observed by SEM.

Table 5 Parameters of the x-ray analysis

Diffracting material	Diffracting plane (*hkl*)	Radiation	Wavelength, Å	Bragg angle 2*θ*, °
Fe-α	(211)	CrKα	λ = 2.29092	156.41

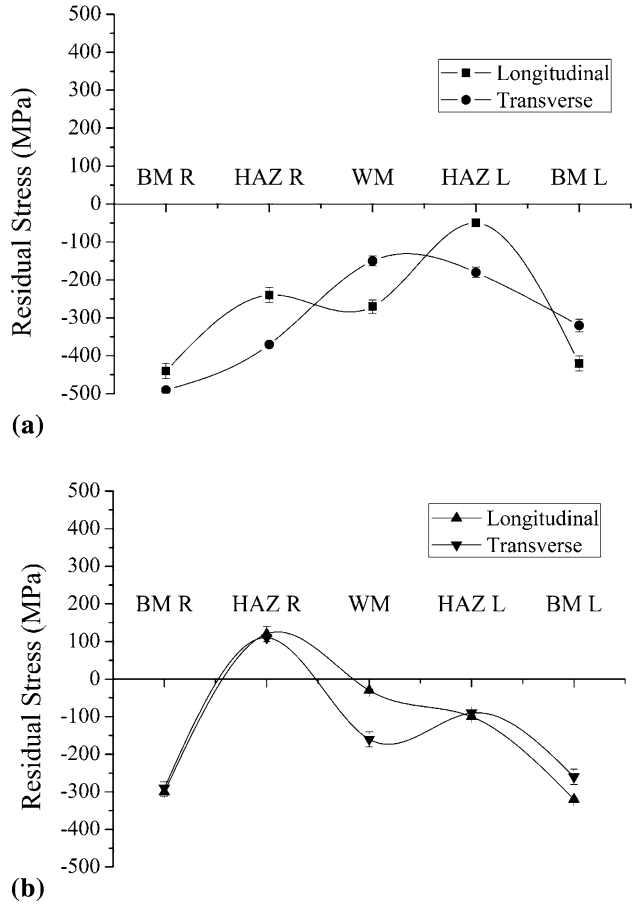

Fig. 3 Residual stress at the top (a) and root (b) of the SMAW welded joint

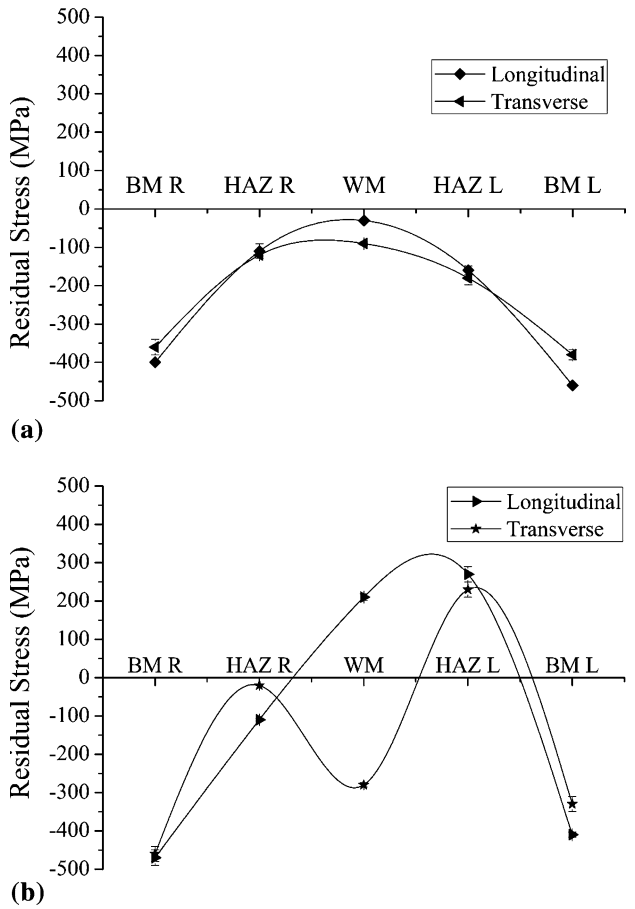

Fig. 4 Residual stress at the top (a) and root (b) of the FCAW welded joint

3. Results and Discussion

3.1 Residual Stress

Figures 3 and 4 show the generated residual stresses in the welded joints by the SMAW and FCAW processes in the longitudinal (*L*) and transverse (*T*) directions at the top and root of the joints. The residual stresses were analyzed in the regions of the right base metal (BM R), right heat-affected zone (HAZ R), weld metal (WM), left heat-affected zone (HAZ L) and left base metal (BM L).

Figures 3(a) and 4(a) show that the residual stresses at the top of the welded joints by the SMAW and FCAW processes are compressive in all analyzed regions. In the root region, residual stresses obtained in the both welding processes were heterogeneous with many compressive regions, but in the some regions were tensile as shown in Fig. 3(b) and Fig. 4(b), including one point in WM of FCAW process root.

Considering that the nature and magnitude of the residual stresses in the welded joints depend not only on the shrinkage process but also on the temperatures differences built up between the near-surface and the core layers of the plate during the cooling of the weld and phase transformations process that occurred during welding, these results are consistent with those reported by Zinn and Scholtes (Ref 15).

Welding processes, as well as the employed consumables, number of passes and deposition rate have a significant effect on the residual stresses, and it can explain the differences between Fig. 3 and 4. Beside that this behavior is coherent with the literature, since in both processes there was the generation of microstructures that alter the specific volume of the weld metal, martensite and bainite, and the rise of thermal stresses due to cooling resulting in the generation of compressive residual stresses (Ref 15-17).

The weld metal with high proportions of columnar regions combined with higher proportion of martensitic microstructure will have higher levels of residual stresses. Also, the microstructural orientation of the weld metal due to the epitaxial growth of the grains leads to higher residual stress on the transversal welding direction.

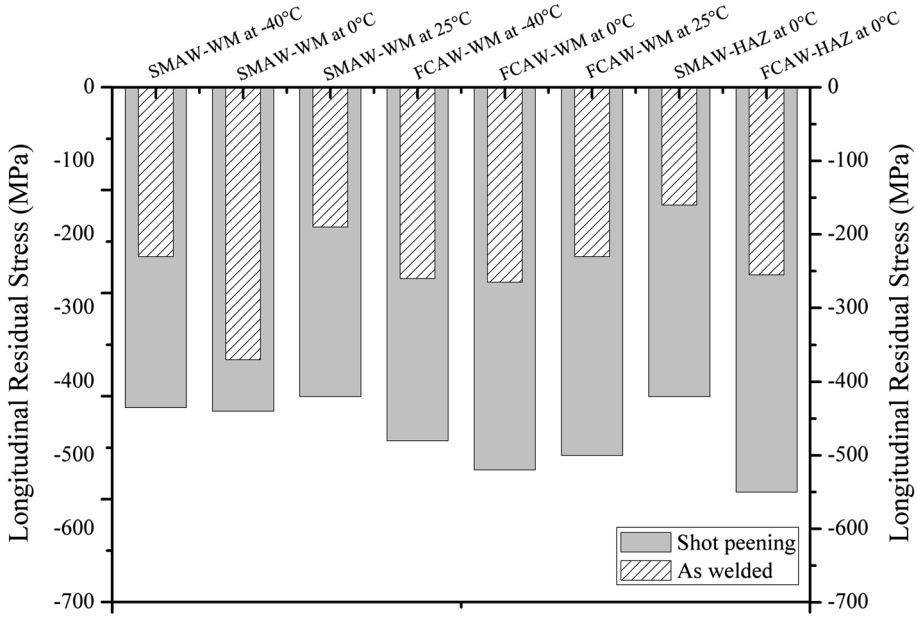

Fig. 5 Longitudinal residual stress in Charpy impact test specimens

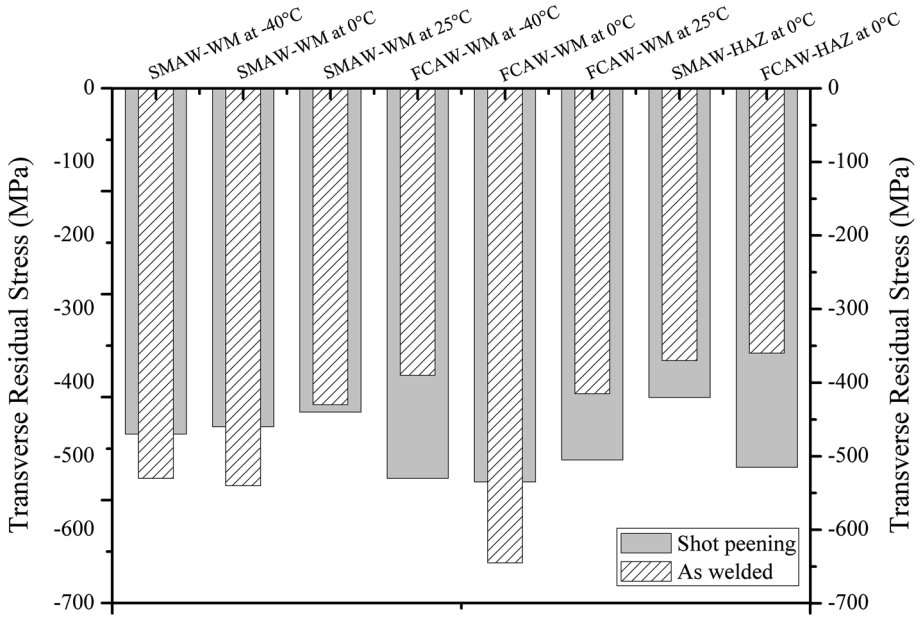

Fig. 6 Transverse residual stress in Charpy impact test specimens

These compressive stress results, which are mainly at the top of the welded joints in both investigated processes, are consistent with those obtained by Araujo et al. (Ref 18), who studied the residual stresses in X80 steel welded joints by the submerged arc welding (SAW) process and found residual stresses of − 250 and 80 MPa; however, in the root, there was a predominance of residual tensile residual stresses. Sowards et al. (Ref 19) observed tensile residual stresses of 30-200 MPa in both directions and regions of X80 steel welded joints obtained by the friction stir welding (FSW) process.

Comparing the results of the present study with those of Araujo et al. (Ref 18) and Sowards et al. (Ref 19), a prevailing compressive residual stress state can be observed, which is beneficial when it increases the fatigue life of the welded structure.

Figures 5 and 6 show the residual stress in the longitudinal (L) and transverse (T) directions, respectively, in welded and shot peening conditions for the Charpy-V test specimens. Figure 7 shows the residual stress longitudinal (L) and transverse (T) directions in the welded and shot peening conditions for the tensile test specimens.

Figures 5, 6 and 7 verify that after the shot peening, the specimens showed an increase in compressive residual stress in both longitudinal and transverse directions. This behavior can be attributed to the surface treatment process, which promotes three important changes on the material surface. First, the

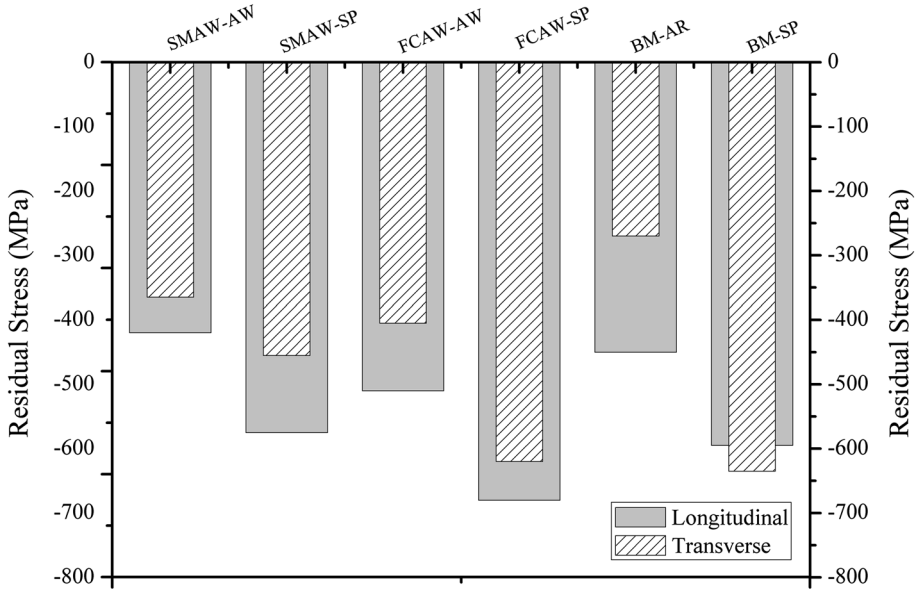

Fig. 7 Residual stress in the welded and shot-peened tensile specimens

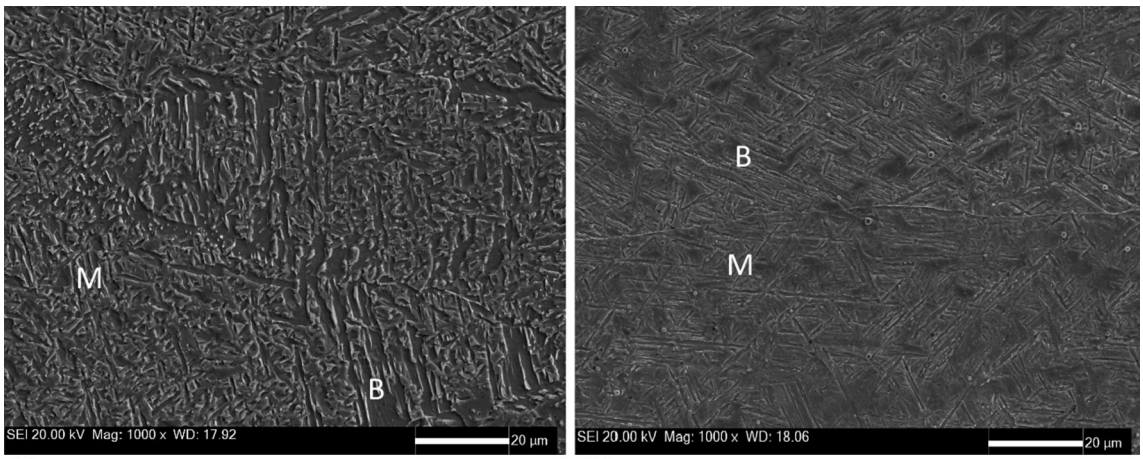

Fig. 8 Microstructures of the top bead of the weld metals (SEM): (a) SMAW and (b) FCAW processes. Etching: nital 2%. B—bainite; M—martensite

surface treatment produces extensive plastic deformation, which results in a structure of unstable dislocations on the surface. These localized damages can accelerate the diffusion of hydrogen, start cracking and promote premature failure. Fortunately, the second change is due to an increase in local deformation resistance that is caused by the strain hardening of the material, which makes the material more resistant to plastic deformation when subjected to loading. The third and most important change in the material is the biaxial compression state, which results from the surface tensile residual stress that the localized plastic deformation produces with lower compensatory tensile (Ref 20).

3.2 Microstructure

Figure 8 shows the microstructure in the top bead of the SMAW and FCAW processes, where it is possible to observe in the top bead of the SMAW process the presence of martensite and bainite, with predominance of bainite while in the top bead of the process FCAW the predominance is of martensite.

Figures 9 and 10 show the microstructure of the columnar and reheated regions of the weld metal of the specimens obtained by the SMAW and FCAW processes, where the notch was positioned for the Charpy-V impact test. It can be noted that the microstructure in both processes consists of martensite and bainite. It is also observed that the microstructure obtained by the FCAW process presents a higher proportion of martensite. This can be explained by the higher cooling rate (Ref 21) observed for the weld metal and the higher carbon equivalent in the weld metal obtained by the FCAW process, increasing the hardenability of the weld metal and generating the grain refinement effect by the formation of a fine martensitic and bainitic microstructure (Ref 22, 23).

According to Ramirez (Ref 22), in weld metals with carbon equivalent of 0.470 or higher, there is the formation of products of low transformation temperature, including martensite. This

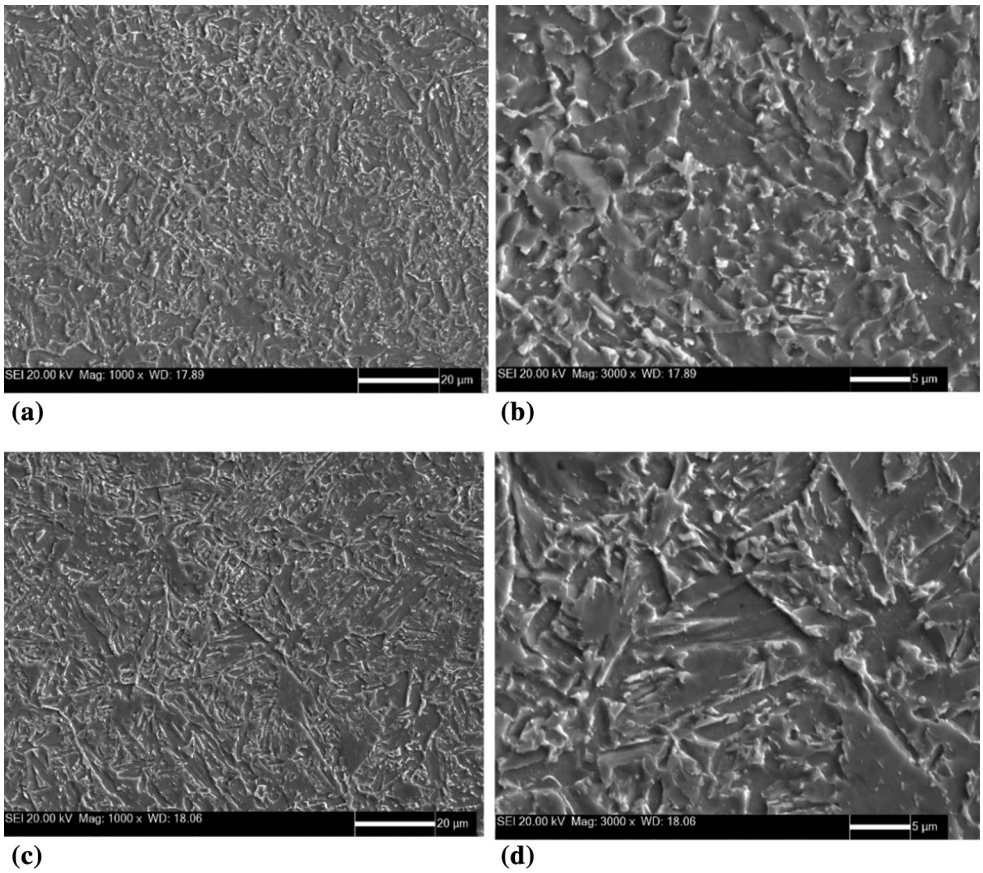

Fig. 9 Microstructures (SEM) of the columnar region: (a) 1000× and (b) 3000× and reheated regions: (c) 1000× and (d) 3000× of the weld metals at SMAW process. Etching: nital 2%

assertion is in agreement with the welding metals observed in the present work, which presented martensite and bainite microstructures, with carbon equivalent of 0.513 and 0.688 for the SMAW and FCAW processes, respectively.

Analyzing the microstructure of the top bead of the weld metals obtained by the SMAW and FCAW processes, Fig. 8, and comparing it with the microstructure present in the columnar and reheated regions of the weld metal, where the notch was positioned for the Charpy-V impact test, for both processes, it is possible to observe that there are no differences between the microstructures present in the top bead and in the region of the Charpy-V notch, since the microstructure observed in the top bead consists of martensite and bainite and in the microstructures of the columnar and reheated regions of the Charpy-V notch in the weld metal the same microstructures are observed, but with higher martensite proportions in the weld metal obtained by the FCAW process due to the lower cooling rate present in this process. Gomes et al. (Ref 23) attribute these changes observed in the microstructures due to small variations in the cooling rates of high-strength weld metals, which is the main reason for the difference observed in the microstructure of the top bead in comparison with the microstructure that is positioned in the notch of Charpy-V impact test specimen that has undergone successive reheats during the multipass welding process. This assumption is in agreement with Lord et al. (Ref 24) results where small variations in the cooling rate of the weld metal can drastically change the transformation temperature and consequently the microstructure of the weld metal.

Another important fact to be observed is the similarity between the microstructures of the columnar and reheated regions of the weld metal for both processes, Fig. 9 and 10, can be explained by the high levels of alloying elements in welding metals not easily retransformed during the heat generated by welding multipass (Ref 22).

3.3 Mechanical Properties

Table 6 and Fig. 11 summarize the tensile testing results of X80 steel (base metal) and welded joints for both processes (SMAW and FCAW). The results are the mean values of 3 specimens for each condition.

The data in Fig. 11 show that the results of both SMAW and FCAW processes were consistent with those observed in the base metal, which is 574 and 675 MPa for the yield and tensile strength, respectively. All specimens showed rupture on the base metal. The FCAW welded joint had the best yield and tensile strength (613 and 690 MPa, respectively).

There was no significant variation of the verified elongation and area reduction in the SMAW and FCAW processes: the elongation was 14 and 18% for the SMAW and FCAW processes.

Comparing the results of the welded joints with the base metal, it is possible to notice that the 35% elongation in the base metal is approximately twice as high, and the area

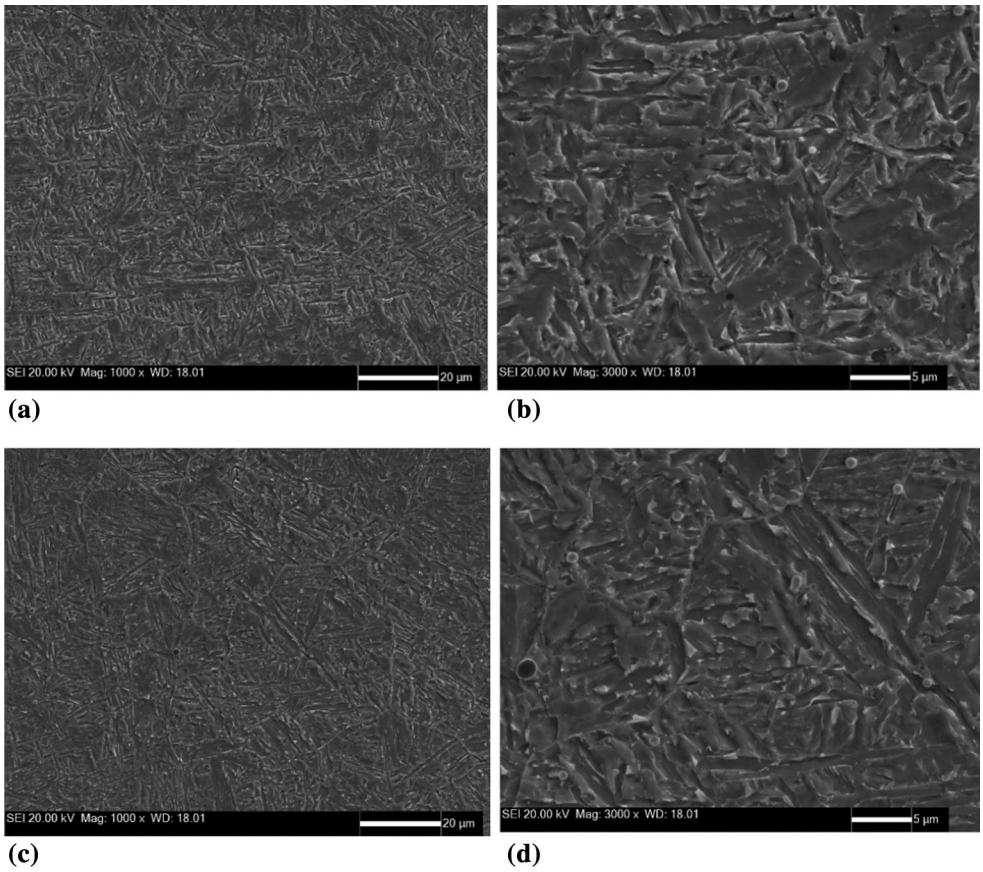

Fig. 10 Microstructures (SEM) of the columnar region: (a) 1000× and (b) 3000× and reheated regions: (c) 1000× and (d) 3000× of the weld metals at FCAW process. Etching: nital 2%

Table 6 Tensile testing results of the base metal and welded joints for SMAW and FCAW processes

Process	Condition	σ_{YS}, MPa	σ_{UTS}, MPa	ε, %
SMAW	As-welded	571	652	14
	Shot peening	623	705	21
FCAW	As-welded	613	690	18
	Shot peening	621	708	20
Base Metal	As-welded	574	675	35
	Shot peening	587	697	30

reduction is 20% smaller than those observed in SMAW and FCAW welded joints. This is probably due to the heterogeneity of the welded joints' material, which consisted of base metal and weld metal, and to the presence of regions that were subjected to different thermal cycles, which was not observed in the results obtained from the base metal, which was subject only to controlled rolling and accelerated cooling in the sheet metal manufacturing process.

The shot peening provided an increase in the tensile strength and yield strength in all conditions (SMAW, FCAW and BM), with a maximum variation of 8% for the tensile strength and 9% for the yield strength in the SMAW condition.

The Vickers microhardness results are shown in Fig. 12(b), (c) and (d) and 13(b), (c) and (d). They were obtained in the regions, Fig. 12(a) and 13(a), that were located at a distance of 3 mm from the surface, HAZ and 3 mm from the root of the welded joints by the SMAW and FCAW processes, respectively.

The welded joint by the SMAW process showed small variations in the Vickers microhardness values in the regions near the top and root of the joint. The HAZ has an average microhardness of 260 HV in the region near the top of the joint and 240 HV in the region near the root. For weld metal, the maximum observed microhardness was 290 HV near the top of the joint, and the range was 260 to 290 HV.

The Vickers microhardness values of the welded joint by the FCAW process were approximately 20% higher than those observed in the SMAW welded joint: 280 and 350 HV in the regions near the surface and between 280 and 345 HV regions near the root.

Figures 12(c) and 13(c) show the Vickers microhardness in the HAZ on the notch position to evaluate the Charpy-V energy

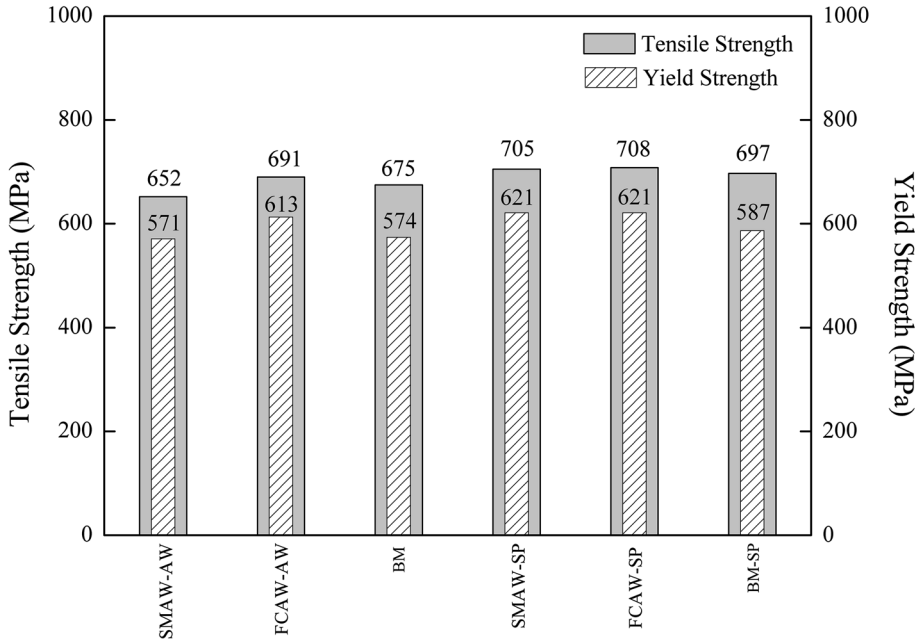

Fig. 11 Tensile testing results of the welded joints of the SMAW and FCAW processes

in the HAZ, where there is no significant variation in the obtained values, and the average Vickers microhardness is 240 and 238 HV for the SMAW and FCAW processes, respectively.

Comparing the results of the SMAW and FCAW welding processes in Fig. 12 and 13, it can be inferred that in both welded joints, there is a small variation of the Vickers microhardness in the weld metal for the region of the measurements: the maximal variations were 30 and 70 HV for the SMAW and FCAW processes, respectively.

The observed difference in the Vickers microhardness shows that both processes can be explained by different chemical compositions of the weld metals and different thermal cycles in the processes.

The weld metal obtained by the FCAW process has a higher equivalent carbon when compared to the SMAW weld metal, so the FCAW weld metal has a higher hardenability and it is possible observed when analyzing the microstructure of this weld metal which has a predominance of martensite, while the SMAW weld metal has a predominance of bainite.

Concerning the thermal cycles, the weld metal obtained by the FCAW process present less reheating than the weld metal obtained by the SMAW process due to welding to obtain the FCAW joint with 12 passes and the welding to obtain the SMAW joint made with 16 passes. The greater number of passes tends to produce a greater proportion of reheated regions reducing the levels of hardness. According to Keehan et al. (Ref 25), the marked reduction of hardness in the reheated regions of high-strength steels weld metals is explained by the formation of precipitates and the loss of carbon from the solid solution during reheating.

Figure 14 compares the microhardness results of the present work (average values) and a collection of results for weld metals of high-strength steels in the welded condition (Ref 22-27). The increase in hardness is directly proportional to the increase in equivalent carbon and consistency of the Vickers microhardness values of the present work with those of the literature.

The average hardness results of the present work are consistent with those observed in the literature for X80 steel weld metal (e.g., Aydin et al. (Ref 4), 333 HV, Sowards et al. (Ref 19), 350 HV, Aquino Filho et al. (Ref 28), 280 HV, Gook et al. (Ref 29), 312 HV, Midawi et al. (Ref 30), 300 HV).

Figure 15 shows the absorbed energy results of the Charpy-V impact tests at 0 °C on the specimens with the notch in the WM and HAZ, as shown in Fig. 1(c) and (d), of the welded joints by the SMAW and FCAW processes.

The impact test results at 0 °C, which were obtained with the notch on the HAZ, of both SMAW and FCAW welded joints presented higher values than those observed in the weld metal. The absorbed energy at 0 °C with the notch in the weld metal of the SMAW and FCAW welded joints was 161 ± 8 and 66 ± 5 J, respectively. The different toughness observed results from weld metals with different chemical compositions, different cooling rates inherent to each welding process and consequently different microstructures. Additionally, it is verified that the weld metal of the FCAW process presents a smaller percentage of reheated region due to the different number of the passes, relative to the weld metal of the SMAW. A higher percentage of reheated region promoted by the greater number of passes during welding results in additional tempering in the microstructure of the previous passes, reducing the internal tensions of the martensitic structures and generating an increase of the toughness.

Figure 16 shows the variation of the absorbed energy in the impact tests at −40, 0 and 25 °C for both welding processes, which verifies that the SMAW weld metals have a higher absorbed energy than do the FCAW weld metals for all temperatures and shot peening. The absorbed energy of the

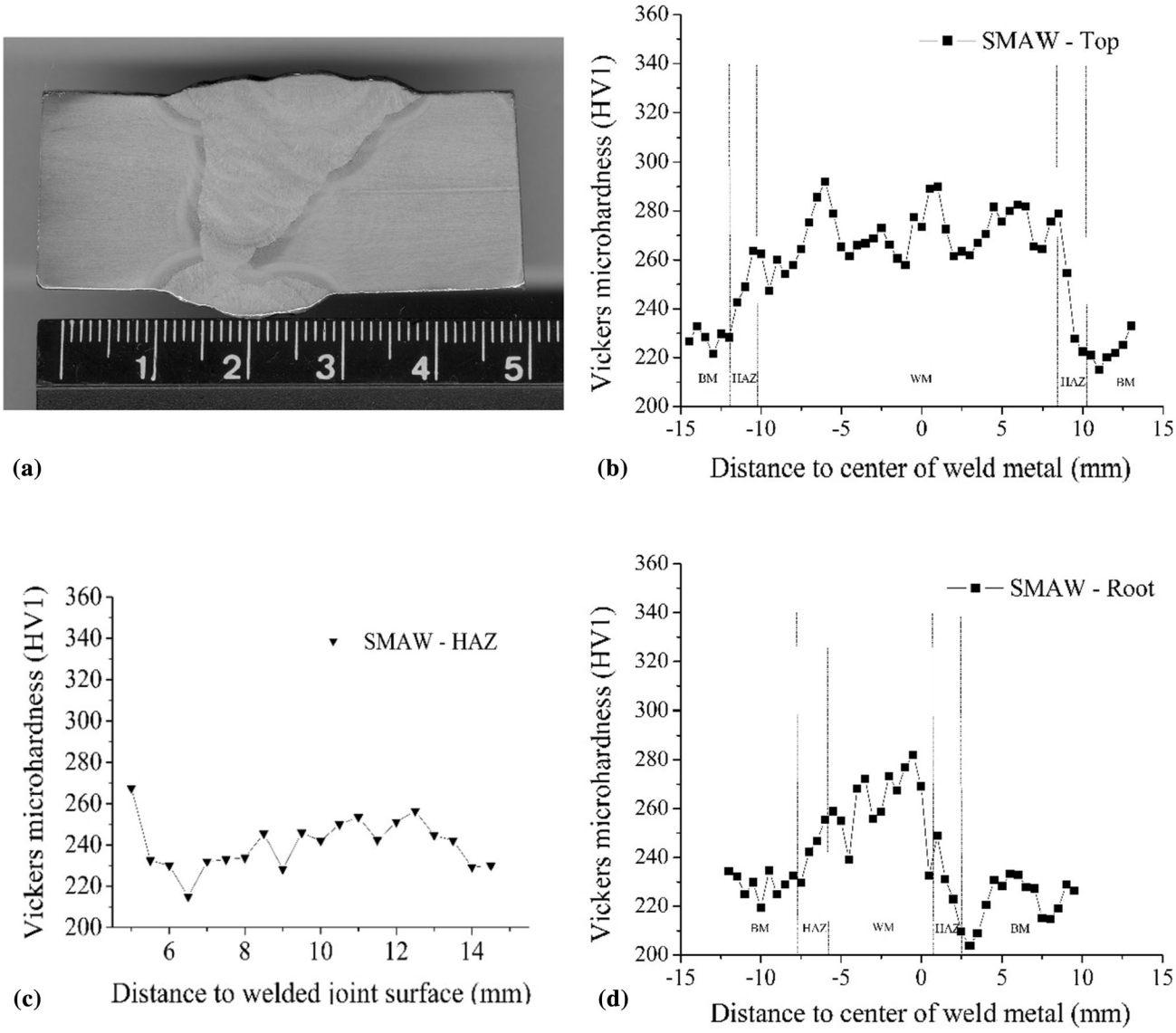

Fig. 12 (a) Macrographic aspect of the joint and Vickers microhardness measurements taken on the (b) top, (c) HAZ and (d) root of the welded joints by the SMAW process

weld metals in both SMAW and FCAW processes increases at − 40 °C, with an increase of 27% in the SMAW process and 41% in the FCAW process.

Comparing the toughness results of the weld metal at 0 °C in the present work with Aquino Filho et al. (Ref 28) and Cooper et al. (Ref 31), who found absorbed energies of 58 and 39 J, respectively, in X80 welded joints by the FCAW process, the results of the present work (66 ± 5 J) are greater than those observed in the literature.

3.4 Fracture Surface Analysis

Figure 17 shows the surface fractures of Charpy-V impact tests of the FCAW welded joint at 0 °C, which were observed with scanning electron microscopy (SEM) to investigate the type of fracture, because the absorbed energy was approximately 41% of that obtained by the SMAW process.

A fracture surface evaluation was performed at the tip of the notch (Fig. 17a and b), where the predominance of dimples,

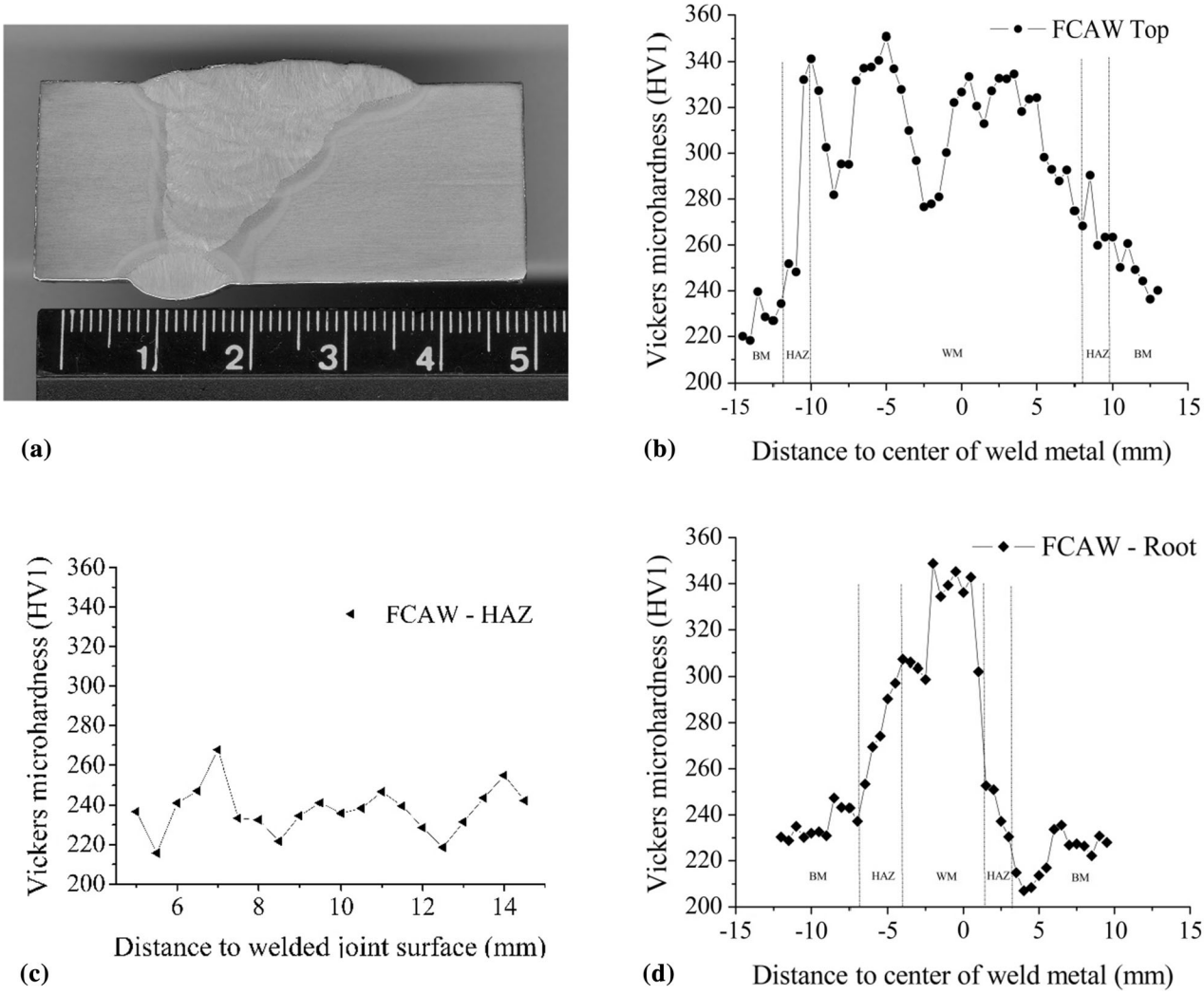

Fig. 13 (a) Macrographic aspect of the joint and Vickers microhardness measurements taken on the (b) top, (c) HAZ and (d) root of the welded joints by the FCAW process

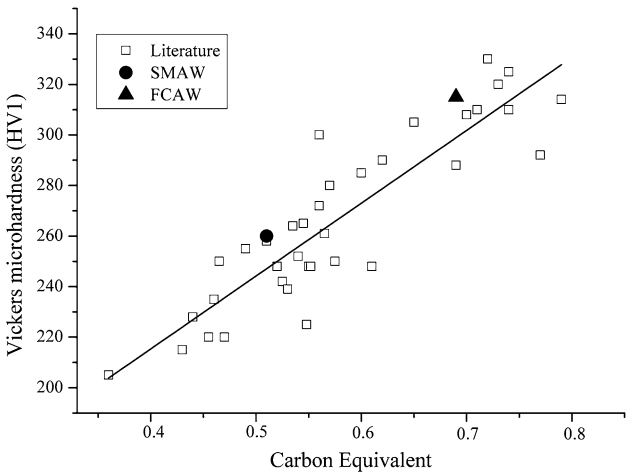

Fig. 14 Relationship between the Vickers microhardness and the carbon equivalent for weld metals in the literature and present work using the SMAW and FCAW processes

which is characteristic of a ductile fracture process, can be verified. At the center of Fig. 17(c) and (d), a mixture of dimples and quasi-cleavage modes of fracture is observed.

4. Conclusions

Whereas the SMAW and FCAW welding processes are widely used in industry, the behavior of high-strength pipe steel X80 welded joints produced by both processes was investigated regarding the mechanical properties and residual stresses. The findings of the study can be summarized as follows:

1. The X80 steel welding joint by the FCAW process exhibits similar mechanical properties to those welded by the SMAW process with respect to tensile strength, but the toughness is high in SMAW process. The differences observed in the toughness values in both processes were the result of the different chemical compositions of the weld metals and the cooling rates inherent to each weld-

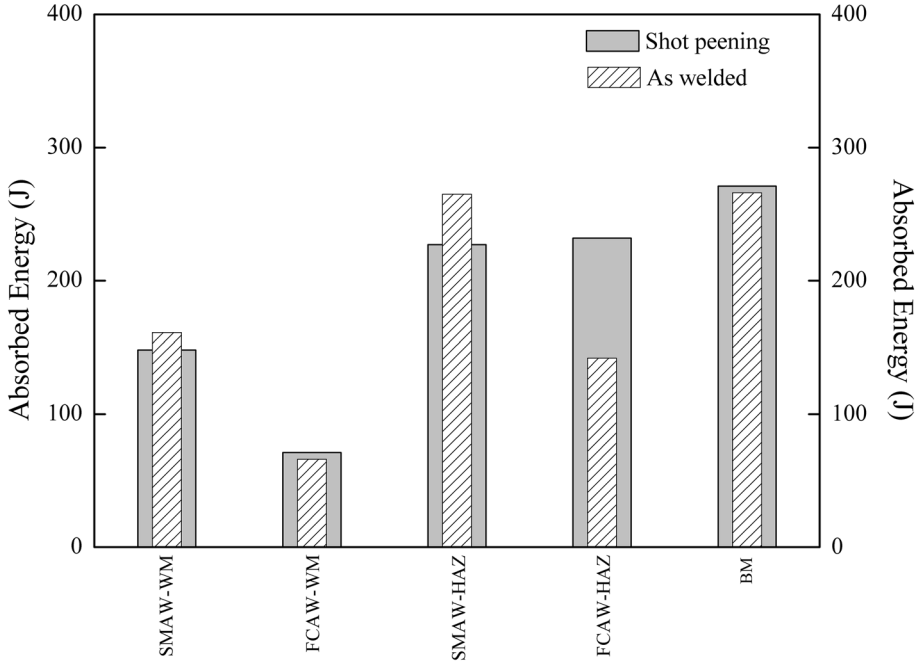

Fig. 15 Absorbed energy of the BM, SMAW and FCAW processes at 0 °C

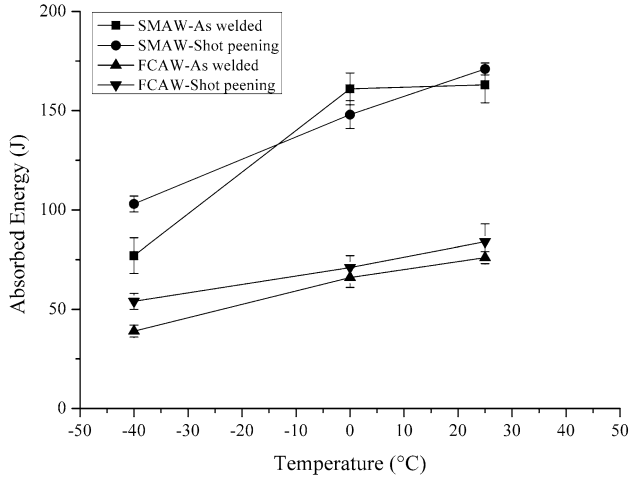

Fig. 16 Absorbed energy vs temperature relationship for FCAW and SMAW weld metals

ing process and that consequently resulted in different microstructures.

2. Microstructures present in the SMAW and FCAW welded joints are composed by martensite and bainite, with predominance of bainite in the SMAW process and martensite in the FCAW process.
3. The residual stresses were predominantly compressive mainly at the top of the joints welded by both processes. This behavior can be explained by microstructural changes that occur in weld metal and modify the specific volume of martensite and bainite, and increase thermal stresses due to cooling resulting in the generation of compressive residual stresses.
4. The contribution of shot peening mechanical treatment on the improvement of tensile and yield strength (27 and 41%, respectively) as well as on the toughness of both welded joints is obvious at high levels of induced compressive residual stresses.

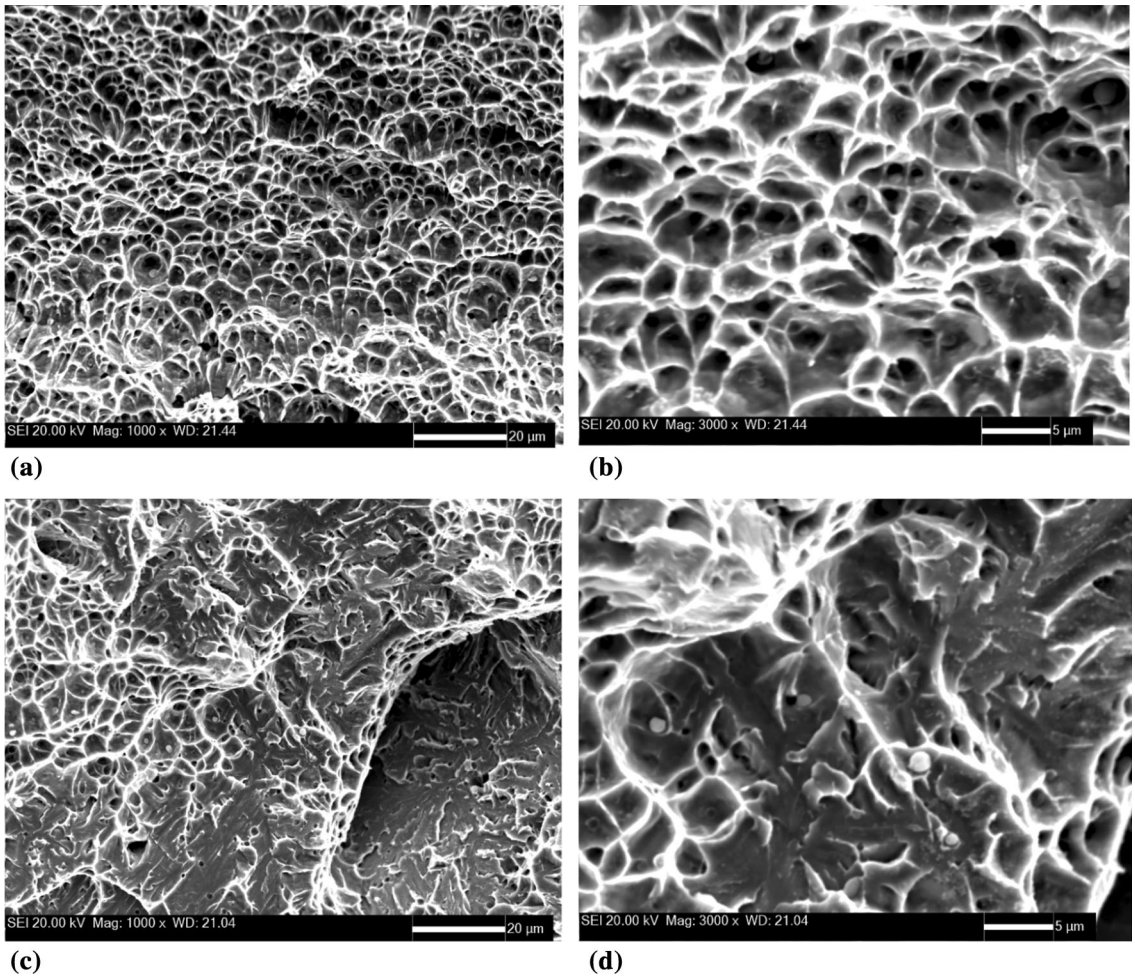

Fig. 17 Fracture surface of the Charpy specimens at the crack initiation region: (a) 1000× and (b) 3000×; at the center of the specimens: (c) 1000× and (d) 3000×

Acknowledgments

The authors would like to thank Brazilian Agencies CNPq, CAPES and FAPERJ for their financial support.

References

1. S.S. Sohn, S.Y. Han, J.H. Bae, H.S. Kim, and S. Lee, Effect of Microstructure and Pipe Forming Strain on Yield Strength Before and After Spiral Pipe Forming of API, X70 and X80 Linepipe Steel Sheets, *Mater. Sci. Eng. A*, 2013, **573**, p 18-23
2. S.Y. Han, S.S. Sohn, S.Y. Shin, J. Bae, H.S. Kim, and S. Lee, Effects of Microstructure and Yield Ratio on Strain Hardening and Bauschinger Effect in Two Linepipe Steels, *Mater. Sci. Eng. A*, 2012, **551**, p 192-199
3. H.I. Yelbay, I. Cam, and C.H. Gür, Non-destructive Determination of Residual Stress State in Steel Weldments by Magnetic Barkhausen Noise Technique, *NDT&E Int.*, 2010, **43**, p 29-33
4. H. Aydin and T.W. Nelson, Microstructure and Mechanical Properties of Hard Zone in Friction Stir Welded X80 Pipeline Steel Relative to Different Heat Input, *Mater. Sci. Eng. A*, 2013, **586**, p 313-322
5. S.E. Khany, M.A. Moyeed, M.S. Siddiqui, G.M.S. Ahmed, and M.M.A. Baig, An Experimental Study of the Effect of Shot Peening on the Low Carbon Steel and Identification of Optimal Process Parameters, *Mater. Today Proc.*, 2015, **2**, p 3363-3370
6. S. Bagheri and M. Guagliano, Review of Shot Peening Processes to Obtain Nanocrystalline Surfaces in Metal Alloys, *Surf. Eng.*, 2009, **25**, p 3-8
7. J. Sakamoto, Y.S. Lee, and S.K. Cheong, Effect of Surface Flaw on Fatigue Strength of Shot-Peened Medium-Carbon Steel, *Eng. Fract. Mech.*, 2015, **133**, p 99-111
8. L. Dieng, D. Amine, Y. Falaise, and S. Chataigner, Parametric Study of the Finite Element Modeling of Shot Peening on Welded Joints, *J. Constr. Steel Res.*, 2017, **130**, p 234-247
9. V. Llaneza and F.J. Belzunce, Optimal Shot Peening Treatments to Maximize the Fatigue Life of Quenched and Tempered Steels, *J. Mater. Eng. Perform.*, 2015, **24**, p 2806-2815
10. N. Habibi, S.M. H-Gangaraj, G.H. Farrahi, G.H. Majzoobi, A.H. Mahmoudi, M. Daghigh, A. Yari, and A. Moridi, The Effect of Shot Peening on Fatigue Life of Welded Tubular Joint in Offshore Structure, *Mater. Des.*, 2012, **36**, p 250-257
11. K. Miková, S. Bagherifard, O. Bokuvka, M. Guagliano, and L. Trsko, Fatigue Behavior of X70 Microalloyed Steel After Severe Shot Peening, *Int. J. Fatigue*, 2013, **22**, p 33-42
12. O. Unal and R. Varol, Almen intensity Effect on Microstructure and Mechanical Properties of Low Carbon Steel Subjected to Severe Shot Peening, *Appl. Surf. Sci.*, 2014, **290**, p 40-47
13. SAE J442, *Test Strip, Holder and Gage for Shot Peening*. January 1995
14. ASTM A 370-05, *Standard Test Methods and Definitions for Mechanical Testing of Steel Products* (2005)
15. W. Zinn and B. Scholtes, Residual Stress Formation Processes During Welding and Joining, *Handbook of Residual Stress and Deformation of Steel*, G. Totten, M. Howes, and T. Inoue, Ed., ASM International, Ohio, 2002, p 391-396
16. E. Macherauch, H. Wohlfahrt, Different Sources of Residual Stress as a Result of Welding, in *Confference on Residual Stresses in Welding Construction and Their Effect*. London, 15-17 Nov 1977, pp. 267-282

17. T.I. Ramjaun, H.J. Stone, L. Karlsson, M.A. Gharghouri, K. Dalaei, R.J. Moat, and H.K.D.H. Bhadeshia, Surface Residual Stress in Multipass Welds Produced Using Low Transformation Temperature Filler Alloys, *Sci. Technol. Weld. Join.*, 2014, **19**(7), p 623-630
18. B.A. Araujo, M.S.S.S. Lima, T.M. Maciel, A.A. Silva, and E.P. Soares, Estudo das Tensões Residuais em Juntas Soldadas de aço API, 5L X80 (Residual Stress Study of API, 5L X80 Steel Welded Joints), *Sold. Insp.*, 2013, **18**(3), p 217-226 (**in Portuguese**)
19. J.W. Sowards, T.G. Herold, J.D. McColskey, V.F. Pereira, and A.J. Ramirez, Characterization of Mechanical Properties, Fatigue-Crack Propagation, and Residual Stresses in a Microalloyed Pipeline-Steel Friction-Stir Weld, *Mater. Des.*, 2015, **88**, p 632-642
20. D.J. Buchanan and R. John, Residual Stress Redistribution in Shot Peened Samples Subject to Mechanical Loading, *Mater. Sci Eng. A*, 2014, **615**, p 70-78
21. E. Keehan, L. Karlsson, and H.-O. Andrén, Influence of Carbon, Manganese and Nickel on Microstructure and Properties of Strong Steel Weld Metal. Part 1—Effect of Nickel Content, *Sci. Technol. Weld. Join.*, 2006, **11**(1), p 1-8
22. J.E. Ramirez, Characterization of High-Strength Steel Weld Metals: Chemical Composition, Microstructure and Nonmetallic Inclusions, *Weld. J.*, 2008, **87**(3), p 65-75
23. A.J.M. Gomes, J.C.F. Jorge, L.F.G. Souza, and I.S. Bott, Influence of Chemical Composition and Post Welding Heat Treatment on the Microstructure and Mechanical Properties of High Strength Steel Weld Metals, *Mater. Sci. For.*, 2013, **758**, p 21-32
24. M. Lord and G. Jennings, Effect of Interpass Temperature on Properties of High-Strength Weld Metals, *Svetsaren*, 1999, **54**(1–2), p 53–58
25. E. Keehan, L. Karlsson, H.-O. Andrén, and K.D.H. Bhadeshia, Influence of Carbon, Manganese and Nickel on Microstructure and Properties of Strong Steel Weld Metal. Part 2—Impact Toughness Gain Resulting from Manganese Reductions, *Sci. Technol. Weld. Join.*, 2006, **11**(1), p 9-18
26. E. Surian, M.R. Rissone, and L. De Vedia, Influence of Molybdenum on Ferritic High Strength SMAW All-Weld-Metal Properties, *Supp. Weld. J.*, 2005, **1**, p 53-62
27. H.G. Rissone, E.S. Svoboda, E. Surian, and L.A. De Vedia, Influence of Procedure Variables on C-Mn-Ni-Mo Metal Cored Wire Ferritic All-Weld-Metal, *Supp. Weld. J.*, 2005, **1**, p 139-148
28. A. Aquino Filho, Y.P. Yadava, and R.A.S. Ferreira, Evenmatched FCAW Process in API, 5L X80 Steel Welded Joints, *Mater. Res.*, 2014, **17**(2), p 295-302
29. S. Gook, A. Gumenyuk, and M. Rethmeier, Hybrid Laser Arc Welding of X80 and X120 Steel Grade, *Sci. Technol. Weld. Join.*, 2014, **19**(1), p 15-24
30. A.R.H. Midawi, E.B.F. Santos, N. Huda, A.K. Sinha, R. Lazor, and A.P. Gerlich, Microstructure and Mechanical Properties in Two X80 Weld Metals Produced Using Similar Heat Input, *J. Mater. Proc. Technol.*, 2015, **226**, p 272-279
31. R. Cooper, J.H.J. Silva, and R.E. Trevisan, Influencia del Precalentamiento em las Propiedades de Uniones Soldadas de Acero API, 5L-X80 Soldadas com Alambre tubular Autoprotegido (Influence of Preheating on API, 5L-X80 Pipeline Joint Welding with Self Shielded Flux Cored Wire), *Ver. Metal.*, 2004, **40**, p 280-287 (**in Spanish**)